nature communications

Article

https://doi.org/10.1038/s41467-025-67503-z

# Persistence of vortexlike phase fluctuations in underdoped to heavily overdoped cuprates

Received: 7 December 2024

Accepted: 2 December 2025

Published online: 16 December 2025

Check for updates

Jasminka Terzic[1,2], Bal K. Pokharel[1,3,6], Zhizhong Li[4], Pascale Senzier[4], Hélène Raffy[4], Shimpei Ono[5] & Dragana Popović[1,3]

The mechanism controlling the superconducting transition temperature $T_c^0$ as a function of doping is a central question in cuprate high-temperature superconductors. While in underdoped cuprates $T_c^0$ is set by global phase coherence rather than the scale of pairing, the role of superconducting phase fluctuations in the overdoped region remains controversial. Here, transport measurements in perpendicular magnetic fields ($H$) on $Bi_{2+x}Sr_{2-x-y}La_yCuO_{6+\delta}$ (Bi-2201) cuprates reveal in the underdoped region immeasurably small Hall response for $T > T_c(H)$ as a signature of a superconducting regime with vortexlike phase fluctuations. The extent of this regime in $T$ and $H$ is suppressed near optimal doping but strongly enhanced in heavily overdoped Bi-2201. These results demonstrate that vortexlike phase fluctuations play a key role in the field-tuned superconducting transition in the heavily overdoped region, in contrast to conventional mean-field Bardeen-Cooper-Schrieffer description. Their unexpected nonmonotonic doping dependence provides a new perspective on the superconducting transition in cuprates.

In copper oxides, superconducting state emerges by doping holes or electrons into an antiferromagnetic (AF) Mott insulator. The doping is accomplished either by varying the oxygen concentration or by substitution with nonisovalent elements, suppressing the AF order of the parent compound, and giving rise to a dome-shaped $T_c^0$ line with increasing concentration of charge carriers ($p$) in the $CuO_2$ planes. In the underdoped region, where $T_c^0(p)$ increases, the superfluid density is low due to the proximity to the Mott insulator[1–3], implying a significant role of superconducting (SC) phase fluctuations. The fluctuations are further enhanced by the effective two-dimensional (2D) nature of underdoped cuprates. As a consequence, the thermodynamic SC transition occurs at $T_c^0$ where long-range phase coherence is established, whereas the onset of SC pairing takes place at some higher, crossover temperature[4]. This is in contrast to conventional superconductors, where the SC transition is well-described by the mean-field Bardeen–Cooper–Schrieffer (BCS) theory, according to which the SC phase coherence and the formation of Cooper pairs occur simultaneously. Within that framework, fluctuations are negligible and, indeed, thermal SC fluctuations are observable within a small temperature range $\delta T$ such that $\delta T/T_c^0 \ll 1$ (ref. 5). On the other hand, the BCS theory was long-believed to provide an adequate description of the cuprate overdoped region, where the number of charge carriers is high and the anisotropy of the material is reduced. However, this view has been challenged recently by several experiments performed at $H = 0$ on heavily hole-doped cuprates[6–9]. Although arguments have been put forward that experimental observations can still be explained within the context of the BCS theory by properly taking into account the inevitable presence of disorder[10,11] ("dirty $d$-wave" theory), others have argued that disorder in a $d$-wave superconductor such as cuprates will lead to an emergent granular SC

[1]National High Magnetic Field Laboratory, Florida State University, Tallahassee, FL, USA. [2]Department of Physics and Astronomy, Western Kentucky University, Bowling Green, KY, USA. [3]Department of Physics, Florida State University, Tallahassee, FL, USA. [4]Laboratoire de Physique des Solides, CNRS, Université Paris-Saclay, Orsay, France. [5]International Center for Synchrotron Radiation Innovation Smart, Tohoku University, Sendai, Japan. [6]Present address: Intel, Hillsboro, OR, USA. e-mail: dragana@magnet.fsu.edu

state[12], implying the importance of phase fluctuations beyond the mean-field treatment. Real-space imaging in $(Pb, Bi)_2Sr_2CuO_{6+\delta}$ (Bi-2201) at $H = 0$ has shown[9] that a state with SC grains embedded in a metallic matrix does indeed develop at high doping, but the results were inconsistent with the BCS theory for spatially heterogeneous systems and also seemed to rule out the effects of thermal phase fluctuations. Therefore, the role of both thermal and quantum phase fluctuations in the overdoped region remains an open question[13].

On the underdoped side, the existence of a broad phase fluctuation regime (at $T > T_c^0$) was widely accepted, but its precise extent in temperature remained a subject of debate for many years[4]. Likewise, in magnetic fields $H$ applied perpendicular to $CuO_2$ planes, the extent of a SC regime with vortices, as well as its interplay with various charge and spin orders, were long controversial, especially at high $H$ as $T \to 0$. Those issues were essentially resolved in a series of linear and nonlinear transport experiments on La-214 cuprates[14–16], which determined the in-plane $T$–$H$ vortex phase diagrams over an unprecedented range of $T$ and $H$. It was shown that the vortex lattice with zero in-plane resistivity ($\rho_{xx} = 0$) is separated from the anomalous high-field normal state by a wide regime of a viscous vortex liquid (VL). In this intermediate field range, the viscous VL freezes into a vortex glass at $T_c(H) = 0$. Thus, at low $T \to 0$, increasing $H$ destroys superconductivity by quantum phase fluctuations[14,16]. At low fields, below the quantum melting field of the vortex lattice where $T_c(H) \to 0$, VL is observable at $T > T_c(H)$ within a temperature range $\delta T(H)$ such that $\delta T(H)/T_c(H) > 1$. Here, including at $H = 0$ (refs. 17,18), thermal phase fluctuations lead to the destruction of superconductivity. These results also demonstrated that the vortex phase diagrams of La-214 underdoped cuprates are qualitatively the same regardless of the type or strength of charge orders[14–16], strongly suggesting that qualitatively the same vortex phase diagrams should apply to all underdoped cuprates. Hence, similar experiments on another cuprate family, preferably one that does not exhibit spin order coexisting with superconductivity in contrast to underdoped La-214, are needed to verify that conclusion. The most important question, though, is whether the VL regime persists to the heavily overdoped regions of the cuprate phase diagram where the (normal state) pseudogap closes.

Therefore, to address the above questions about the role of SC phase fluctuations, here we focus on doped $Bi_2Sr_2CuO_6$ (i.e., Bi-2201), which has several properties that make it an ideal system for this study. Bi-2201 has a simple single-band Fermi surface and, using the chemical substitution or by varying the oxygen concentration, the parent compound can be easily doped all the way to the edge of the SC dome without undergoing Lifshitz transitions[19]. Just like La-214, Bi-2201 has a single $CuO_2$ layer per unit cell, and its relatively low $T_c^0$ allows us to fully suppress superconductivity with $H$ and probe deep into the field-revealed normal state. Bi-2201 has a relatively large residual resistivity[20–23], suggesting the importance of disorder, and in contrast to La-214, only short-range charge order has been reported[24–26], with no evidence of spin order[27]. We combine linear in-plane resistivity $\rho_{xx}$ and Hall resistivity $\rho_{yx}$ with nonlinear in-plane transport or voltage–current ($V$–$I$) characteristics to probe both charge and vortex matter over a wide range of $10^{-2} \lesssim T/T_c^0 \lesssim 10$ down to mK temperatures and fields up to $H/T_c^0 \gtrsim 10$ T/K for several values of doping (Fig. 1a). Our main results are summarized in Fig. 1b-e. In the underdoped region, we find that, qualitatively, the $T$–$H$ vortex phase diagram (Fig. 1b) is the same as that in the La-214 family[14–16] and, thus, independent of the presence of spin order. This result establishes the universality of the vortex phase diagram in underdoped cuprates. Using complementary transport techniques allows us also to reveal a vanishing Hall response ($\rho_{yx} = 0$) as a signature of the viscous VL regime in which $\rho_{xx} \neq 0; \rho_{yx} = 0$ is thus attributed to the increasing viscosity of the vortex motion with decreasing $T$. By tracking the evolution of such a regime with doping (Fig. 1c, d), we obtain our key results. First, the VL does persist in the heavily overdoped region, such that it is observable up to $\delta T(H)/T_c(H) > 1$ (Fig. 1d, e). Therefore, complementing previous $H = 0$ studies[6–9] that used other techniques, our magnetotransport measurements indicate that the SC transition in heavily overdoped cuprates is of a non-mean-field type. Second, in contrast to a commonly held belief, the doping dependence of $\delta T(H)/T_c(H)$ is non-monotonic (Fig. 1e): vortexlike excitations are considerably suppressed near optimal doping compared to both underdoped and heavily overdoped regions.

## Results

### Underdoped region

Underdoped Bi-2201 samples are single crystals of $Bi_2Sr_{2-x}La_xCuO_{6+\delta}$ with $x = 0.84$ and $p = 0.10 \pm 0.02$ (see "Methods"). Similar to earlier measurements[28] of the in-plane resistivity down to $T = 0.7$ K, our study down to much lower ~0.05 K finds that $\rho_{xx}(H)$ at low enough $T$ increases (Fig. 2a), indicating a suppression of superconductivity by $H$. This is followed by a weak field dependence of $\rho_{xx}$ at higher $H$, representing the normal-state behavior. The $\rho_{xx}(H)$ data were used to determine $T_c(H)$, the melting temperature of the vortex lattice in which $\rho_{xx} = 0$, as well as $H_c'(T)$, the onset of Gaussian fluctuations of the SC amplitude and phase. As usual[14,16,29,30], $H_c'(T)$ is defined as the field above which the magnetoresistance increases as $H^2$, as expected in the high-$T$ normal state (Supplementary Fig. 1).

At the highest $T$, the Hall resistivity $\rho_{yx} \propto H$, as expected in conventional metals (Fig. 2b; see also Supplementary Fig. 2a–d for measurements up to 41 T, Supplementary Figs. 3a–d for the corresponding Hall coefficient $R_H = \rho_{yx}(H)/H$, as well as Supplementary Fig. 4 for $\rho_{yx}(H)$ and $R_H(H)$ at various $T$.) At lower $T$, as $H$ increases and suppresses superconductivity, the Hall signal increases and then recovers its conventional $\rho_{yx} \propto H$ behavior at high $H$ (Supplementary Figs. 2a–d), i.e., $R_H$ becomes independent of the field (Supplementary Figs. 3a–d; also Supplementary Fig. 4). The results are in good agreement with previous Hall measurements in underdoped Bi-2201, which focused on exploring the Hall coefficient in the normal state[31]. Here, in contrast, we focus on the low-field regime, where $\rho_{yx}$ starts to deviate from zero. Surprisingly, we observe a large, up to several teslas, difference in the onset fields of nonzero $\rho_{xx}$, which defines $T_c$ for that field, and nonzero $\rho_{yx}$ (Fig. 2b inset). $T_{R_H=0}(H)$, i.e., the onsets of $\rho_{yx} = 0$ or $R_H = 0$, are also shown in the $\rho_{xx}(T)$ data for various fields (solid line in Fig. 2c). Following their initial suppression by increasing $H$, $T_{R_H=0}(H)$ appear to track $T_{peak}(H)$, the position of the peak in $\rho_{xx}(T)$, which emerges at intermediate fields. In underdoped La-214 cuprates, $T_{peak}(H)$ was identified[14,16] as the onset of the viscous VL observed at $T < T_{peak}(H)$. From the $T$–$H$ phase diagram in Fig. 1b, it is obvious that there is a fairly wide regime with $\rho_{xx} \neq 0$ and $R_H = 0$ observed at $T > T_c$ for a given $H$, which is distinct from the pinned vortex lattice characterized by $\rho_{xx}(T < T_c) = 0$ and $R_H = 0$. At low $T$, the boundary of the $R_H = 0$ regime indeed approaches $T_{peak}(H)$.

To confirm the existence of the viscous VL at intermediate fields, between $T_c(H)$ and $T_{peak}(H)$, we use two methods. First, we consider the $T$-dependence of the linear ($I_{dc} \to 0$) resistivity $\rho_{xx}(T)$. We establish that, for $T < T_{peak}(H)$, it is described best with the power-law fits $\rho_{xx}(H, T) = k(H)T^{\alpha(H)}$, where $\alpha(H)$ decreases to zero with $H$ (Supplementary Fig. 5a, b). The power-law dependence suggests that, at intermediate fields, a true SC state ($\rho_{xx} = 0$) exists only at $T = 0$ when the vortices are frozen. Similar behavior was found[14,16] in underdoped La-214 cuprates, consistent with the expectations for a viscous VL above its glass freezing temperature[32–34] $T_g = 0$. Second, we measure nonlinear transport, i.e., differential resistance $dV/dI$ as a function of the dc current excitation $I_{dc}$ ("Methods"). In the same field range at low $T$, we find that $dV/dI$ is non-Ohmic for $I_{dc} \neq 0$, although the linear resistance ($dV/dI$ for $I_{dc} \to 0$) is not zero (Supplementary Fig. 5c, d). This type of behavior is precisely what is expected from the motion of vortices in the presence of disorder, i.e., it is a signature of a viscous VL[35]. At higher $H$, Ohmic behavior is recovered (Supplementary

https://doi.org/10.1038/s41467-025-67503-z

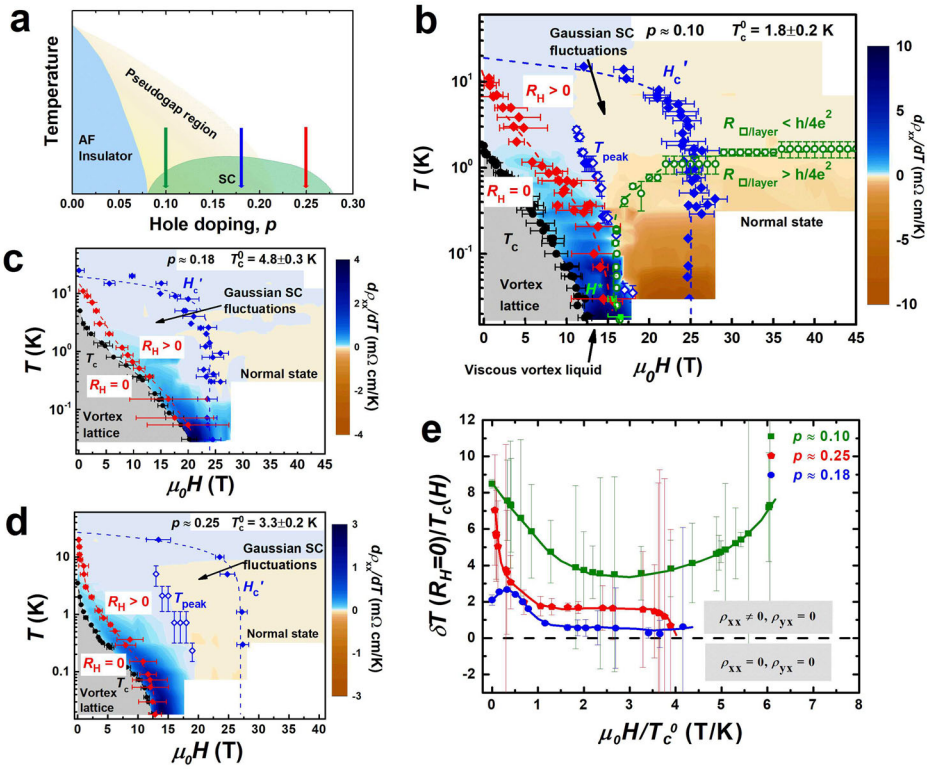


**Fig. 1 | In-plane transport in Bi-2201 cuprates. a** $T$-$p$ phase diagram with the antiferromagnetic (AF) phase, SC dome, and the pseudogap region shown schematically. The arrows show the doping values of the Bi-2201 samples with the corresponding $T$-$H$ phase diagrams ($H \| c$) given in (**b**, **c**, **d**). **b**, **c**, **d** Color map: $d\rho_{xx}/dT$. Solid blue diamonds: $H_c'(T)$, the fields above which Gaussian SC fluctuations are not observed. The error bars for $H_c'(T)$ correspond to ±1 SD (standard deviation) in the slopes of the linear fits in Supplementary Fig. 1. The dashed lines are fits with $\mu_0 H_c'$ [T] = (25 ± 2)[1 − (T[K]/(18.9 ± 0.9)$^2$], $\mu_0 H_c'$ [T] = (24 ± 3)[1 − (T[K]/(19 ± 2)$^2$], and $\mu_0 H_c'$ [T] = (27 ± 1)[1 − (T[K]/(26.9 ± 0.7)$^2$], respectively. Black dots: $T_c(H)$; $T_c(H) \to 0$ at ~12.8 T in (**b**). Red diamonds: $T_{R_H=0}(H)$, boundary between the regime with $R_H > 0$, found at higher $H$ and $T$, and the $R_H = 0$ regime; the dashed red line guides the eye. The error bars for $T_c(H)$ and $T_{R_H=0}(H)$ represent the uncertainty in determining the magnetic field at which resistance and Hall resistance, respectively, rise by 1 SD above the 0.7 mΩ resistance noise floor. Open blue diamonds in (**b**, **d**): $T_{peak}(H)$, a position of the peak in $\rho_{xx}(T)$ for a given $H$. The error bars represent the uncertainty in the zero intercept of the $d\rho_{xx}/dT$ curve. **b** $H^*(T)$ (light green squares): boundary between the viscous VL with non-Ohmic $dV/dI$ for $H < H^*(T)$ and Ohmic behavior at $H > H^*(T)$. The error bars reflect the uncertainty in determining $H^*(T)$ for data taken in steps of 1 T. Open green circles separate the low-$T$, high-$H$ regime where $R_{\square/layer} > R_Q$ from the regime where $R_{\square/layer} < R_Q$. The error bars reflect a ±1 SD of $R_{\square/layer}$ away from $h/4e^2$. **e** $\delta T(R_H = 0)/T_c(H) = [T_{R_H=0}(H) - T_c(H)]/T_c(H)$ from **b**, **c**, and **d** vs $\mu_0 H/T_c^0$. $\delta T(R_H = 0)$ were calculated from the fits of $T_c(H)$ and $T_{R_H=0}(H)$ to an exponential form, respectively, and the error bars for $\delta T(R_H = 0)/T_c(H)$ result from ±1 SD in those fits.

Fig. 5d), allowing us to determine fields $H^*(T)$ that separate the viscous VL regime at lower $H$ from the Ohmic regime characteristic of the normal state at high $H$ (Fig. 1b). Just like in underdoped La-214 cuprates[14,16], as $T \to 0$ there is a quantitative agreement between $H^*(T)$, the boundary of the viscous VL obtained from nonlinear transport, with the values of $T_{peak}(H)$ obtained from the linear resistivity measurements. Moreover, here these two characteristic energy scales, which indicate the vanishing of the SC regime with vortices, also follow the "$h/4e^2$" line (Fig. 1b), where the sheet resistance $R_{\square/layer} \approx R_Q$, with $R_Q = h/(2e)^2$ the quantum resistance for Cooper pairs. This suggests the onset of localization of Cooper pairs in $CuO_2$ planes[36] at $T = 0$, i.e., a quantum phase transition from a frozen viscous VL (vortex glass) to the well-known, albeit little-understood anomalous normal state (Fig. 1b) with a weak, insulating $\rho_{xx} \propto ln(1/T)$ behavior[28,37] for $H > H_c'$ (Fig. 2c). Therefore, by using complementary transport techniques that are sensitive to global phase coherence, we have established that $R_H = 0$ with $\rho_{xx} \neq 0$ clearly represents a signature of the SC regime with vortexlike phase fluctuations.

Our results demonstrate that the vortex phase diagram in underdoped Bi-2201 ($p = 0.10 \pm 0.02$) is qualitatively the same as that in the La-214 family and, thus, independent of the details of either spin or charge orders. This universality observed in the underdoped region is further supported by $\rho_{xx}$ vs $I$ measurements[38] in Bi-2201 with $p \approx 0.125$ for $\mu_0 H/T_c^0 \approx 1.2$ and $YBa_2Cu_4O_8$ with $p = 0.14$ for $\mu_0 H/T_c^0 \approx 0.6$, which provided evidence for the presence of a vortex liquid. Furthermore, we show that Hall effect measurements and, in particular, the regime with $R_H = 0$ and $\rho_{xx} \neq 0$, can be used to identify the presence of a viscous vortex liquid in Bi-2201. Therefore, we focus on this method, employed along other transport techniques, to determine vortex phase diagrams in Bi-2201 at higher doping, all the way to the heavily overdoped region.

## Weakly overdoped region

Weakly overdoped Bi-2201 samples are single crystals of $Bi_{2.1}Sr_{1.9}CuO_{6+\delta}$ with hole concentration $p = 0.18 \pm 0.02$ (see "Methods"). As in the underdoped region, we measure $\rho_{xx}(H)$ and $\rho_{yx}(H)$ at different $T$ [Fig. 3a, b, respectively; see also Supplementary Figs. 2e–h for additional $\rho_{yx}(H)$ data, i.e., Supplementary Figs. 3e–h for the corresponding $R_H(H)$]. Here we also observe a clear difference in the onset fields of nonzero $\rho_{xx}$ and nonzero $\rho_{yx}$ (Fig. 3b inset). The onsets of $R_H = 0$ are shown in the $\rho_{xx}(T)$ data for various fields (solid line in Fig. 3c), as well as in the $T$–$H$ phase diagram (Fig. 1c).

It is apparent that the regime with $R_H = 0$ and $\rho_{xx} \neq 0$, indicative of the viscous VL, is substantially suppressed compared to the underdoped region (cf. Figs. 2c and 1b), in agreement with general expectations[2]. In particular, here $R_H = 0$ with $\rho_{xx} \neq 0$ is observed only at

https://doi.org/10.1038/s41467-025-67503-z

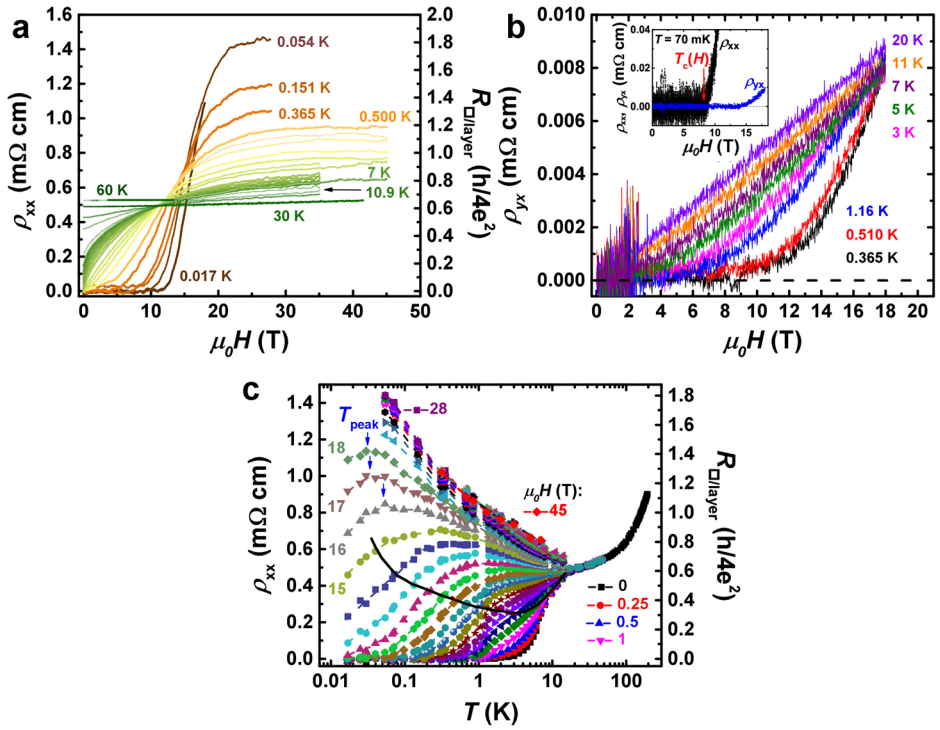


**Fig. 2 | In-plane magnetotransport in underdoped Bi-2201 ($p$ = 0.10 ± 0.02).** **a** $\rho_{xx}$ vs $H\|c$ at several $T$, as shown. Right axis: the corresponding $R_{\square/layer}$ in units of quantum resistance for Cooper pairs, $R_Q = h/4e^2$. **b** $\rho_{yx}$ vs $H$ up to 18 T at several $T$, as shown. Inset: Difference in the onsets of nonzero $\rho_{yx}$ (blue curve) and $\rho_{xx}$ (black curve) at $T$ = 0.07 K; red arrow indicates $T_c(H)$, i.e., the onset of nonzero $\rho_{xx}$. **c** $\rho_{xx}(T)$ for several $H$ up to 45 T; the data for 1≤$H$(T)≤45 are shown in steps of 1 T. Blue arrows indicate the peak in $\rho_{xx}(T)$, $T_{peak}(H)$; right axis: the corresponding $R_{\square/layer}$. Solid black line guides the eye to show $T_{R_H=0}(H)$, the onset of zero Hall coefficient, for 0.25≤$H$[T] ≤15.

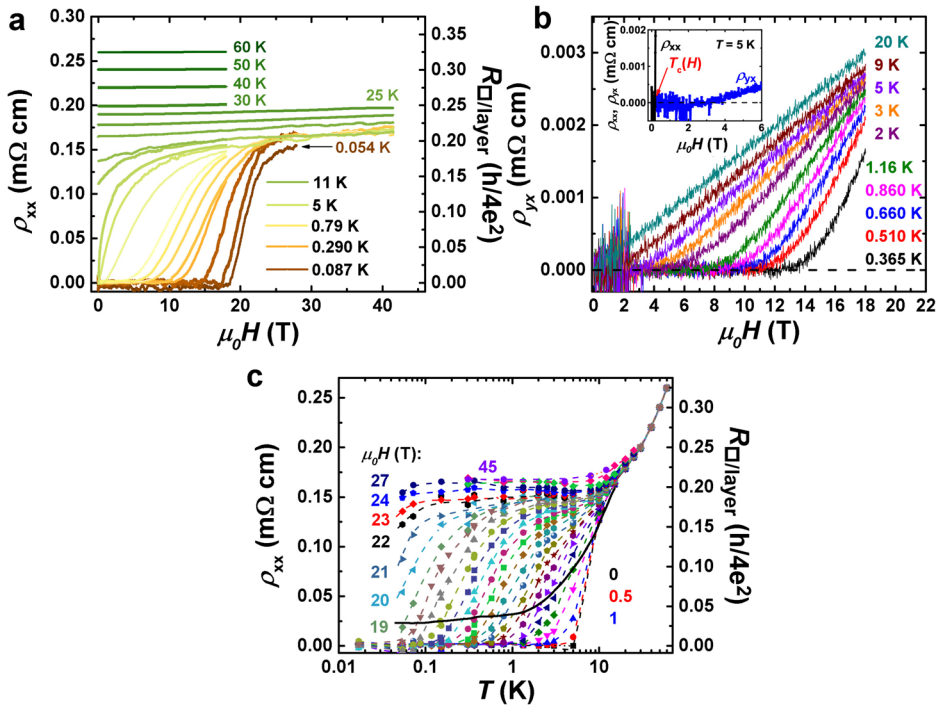


**Fig. 3 | In-plane magnetotransport in weakly overdoped Bi-2201 ($p$ = 0.18 ± 0.02).** **a** $\rho_{xx}$ vs $H\|c$ at several $T$, as shown. Right axis: the corresponding $R_{\square/layer}$ in units of quantum resistance for Cooper pairs, $R_Q = h/4e^2$. **b** $\rho_{yx}$ vs $H$ up to 18 T at several $T$, as shown. Inset: Difference in the onsets of nonzero $\rho_{yx}$ (blue curve) and $\rho_{xx}$ (black curve) at $T$ = 5 K; red arrow indicates $T_c(H)$, i.e., the onset of nonzero $\rho_{xx}$. **c** $\rho_{xx}(T)$ for several $H$ up to 45 T, as shown; the data for 1≤$H$(T)≤19 are given in steps of 1 T, while the highest $H$ curves correspond to 45 T, 38 T, and 35 T, respectively. The right axis shows the corresponding $R_{\square/layer}$. Solid black line guides the eye to show $T_{R_H=0}(H)$, the onset of zero Hall coefficient, for 0.5≤$H$[T] ≤19.

https://doi.org/10.1038/s41467-025-67503-z

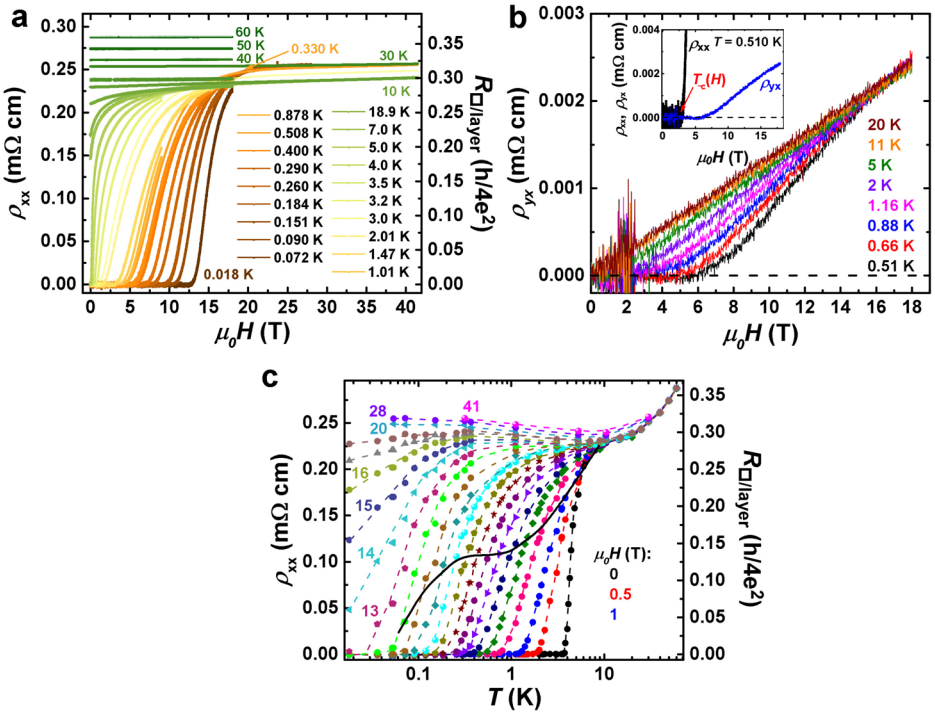


**Fig. 4 | In-plane magnetotransport in heavily overdoped Bi-2201 ($p$ = 0.25 ± 0.01). a** The in-plane longitudinal resistivity $\rho_{xx}$ vs $H \| c$ at several $T$, as shown. The right axis shows the corresponding $R_{\square/layer}$ in units of quantum resistance for Cooper pairs, $R_Q = h/4e^2$. **b** Hall resistivity $\rho_{yx}$ vs $H$ up to 18 T at several $T$, as shown. Inset: Difference in the onsets of nonzero $\rho_{yx}$ (blue curve) and $\rho_{xx}$ (black curve) at $T$ = 0.510 K; red arrow indicates $T_c(H)$, i.e., the onset of nonzero $\rho_{xx}$. **c** $\rho_{xx}(T)$ for several $H$ up to 41 T, as shown; the data for $1 \le H(T) \le 18$ are shown in steps of 1 T. The right axis shows the corresponding $R_{\square/layer}$. Solid black line guides the eye to show $T_{R_H=0}(H)$, the onset of zero Hall coefficient, for $0.5 \le H[T] \le 12$.

lower $H \lesssim 20$ T, i.e., for $T > T_c(H)$ (Fig. 1c). In this range of fields, $\rho_{xx}(T)$ (Fig. 3c; also Supplementary Fig. 6) is more reminiscent of the behavior of a BCS-type superconductor, indicating relatively weak thermal SC fluctuations. At intermediate fields $20 \lesssim H[T] \lesssim H'_c(T=0) = 24$ where Gaussian SC fluctuations are still observed (Fig. 1c) a peak in $\rho_{xx}(T)$ is not found at low $T$ (Fig. 3c). Instead, at these fields at the lowest $T < 0.1$ K, $\rho_{xx}$ seems to drop with decreasing $T$ in a manner similar to that at low fields for $T > T_c(H)$ (Supplementary Fig. 6), in contrast to the behavior in the underdoped region (Supplementary Fig. 5a, b). In addition, nonlinear $dV/dI$ was not observed either, suggesting the absence of a viscous VL at intermediate fields. Current-dependent $\rho_{xx}$ was also not observed[38] in $Bi_2Sr_{2-x}La_xCuO_{6+\delta}$ with $p \approx 0.19$ for $\mu_0 H/T_c^0 \approx 1.3$. Finally, at the highest fields [$H > H'_c(T=0) = 24$ T] where SC fluctuations are no longer observed, the $T$-dependence of $\rho_{xx}$ is negligible, indicative of the metallic normal state, in agreement with the Hall effect measurements (Supplementary Fig. 7) and previous work[28].

## Heavily overdoped region

Heavily overdoped Bi-2201 samples are thin films of $Bi_2Sr_2CuO_{6+\delta}$ (see "Methods"). Here $\rho_{xx}(H)$ and $\rho_{yx}(H)$ measurements at different $T$ on a film with $p$ = 0.25 ± 0.01 [Fig. 4a, b, respectively; see also Supplementary Figs. 2i–l for additional $\rho_{yx}(H)$ data, i.e., Supplementary Figs. 3i–l for the corresponding $R_H(H)$] also reveal a large difference in the onset fields of nonzero $\rho_{xx}$ and nonzero $\rho_{yx}$ (Fig. 4b inset), i.e., a regime with $R_H = 0$ and $\rho_{xx} \neq 0$ observed over a wide range of $T > T_c(H)$ and $H < 13$ T (Figs. 4c and 1d). Surprisingly, the suppression of this regime by $H$ (solid line in Fig. 4c) seems to occur less rapidly than in the weakly overdoped region (cf. solid line in Fig. 3c).

At intermediate fields (13 T $\lesssim H \lesssim$ 19 T), a peak in $\rho_{xx}(T)$ emerges (Fig. 4c). Although not as pronounced as in the underdoped region (Fig. 2c), here we also find a power-law dependence characteristic of a viscous VL: $\rho_{xx}(H,T) = k(H)T^{\alpha(H)}$ for $T < T_{peak}(H)$, with $\alpha(H)$ decreasing to zero with $H$ (Supplementary Fig. 8). While any nonlinear $dV/dI$ was too weak to be observed in this sample, the peak in $\rho_{xx}(T)$ becomes more pronounced with further increase in doping (see Supplementary Fig. 9 for a film with $p$ = 0.27 ± 0.01). This confirms the presence of the intermediate viscous VL regime in heavily overdoped samples, outside of the pseudogap regime, and its nonmonotonic dependence on doping.

At the highest fields $H > H'_c(T=0) \sim 27$ T where SC fluctuations are fully suppressed (Fig. 1d), the normal-state $\rho_{xx}(T)$ is weak, indicative of a metallic ground state, with $d\rho_{xx}/dT < 0$ suggesting the effects of disorder. These findings are also in agreement with our Hall effect measurements (Supplementary Fig. 10). Moreover, we note that the high-field, normal-state value of $R_H$ obtained on the $p$ = (0.25 ± 0.01) $Bi_2Sr_2CuO_{6+\delta}$ film for $T \to 0$ (Supplementary Fig. 10b) is comparable to that found[21] at higher $T$ = (15 − 54) K on a $Bi_{2-y+x}Pb_ySr_{2-x}CuO_{6+\delta}$ single crystal with a similar $p \approx 0.245$, thus demonstrating consistent behavior between films and single crystals.

## Evolution of vortexlike phase fluctuations with doping

To examine the dependence of the $R_H = 0$, $\rho_{xx} \neq 0$ regime on doping, we analyze its extent in $T$ above $T_c(H)$, i.e., its relative width $\delta T(R_H=0)/T_c(H) = [T_{R_H=0}(H) - T_c(H)]/T_c(H)$ for fixed $H$ for the values of $p$ that we have studied in detail (Fig. 1a). Figure 1e shows that, in the underdoped region at low $H$, the relative width of the viscous VL, as determined from $R_H = 0$ with $\rho_{xx} \neq 0$, extends even up to $\delta T(H)/T_c(H) \sim 7$, consistent with the findings in underdoped La-214 cuprates using different probes of vortex matter (refs. 14,16,39 and refs. therein). Following its initial suppression by $H$, $\delta T(H)/T_c(H)$ increases to comparably large values [$\delta T(H)/T_c(H) \sim 8$] at high fields, reflecting the presence of the viscous VL at $T < T_{peak}(H)$ (see Fig. 2c and Fig. 1b). We recall that the viscous VL with $T_c(H) = 0$ (vortex glass) persists to even higher $H \approx H^*$ (Fig. 1b, not shown in Fig. 1e), a regime where quantum phase fluctuations dominate as $T \to 0$ similar to underdoped La-214

cuprates[14,16]. In the weakly overdoped region, the $R_H = 0$, $\rho_{xx} \neq 0$ regime is considerably smaller (Fig. 1e), with $\delta T(H)/T_c(H) < 1$ at higher fields, indicating that here vortexlike phase fluctuations do not play an important role in the field-tuned destruction of superconductivity. In the heavily overdoped region, on the other hand, $\delta T(H)/T_c(H)$ at the lowest $H$ is almost as large as in the underdoped region, but it is then quickly suppressed by the field (Fig. 1e). However, it remains much larger than in the weakly overdoped region for all $H$. In particular, $\delta T(H)/T_c(H) \sim 2$, indicating that the SC transition in heavily overdoped Bi-2201 cannot be described within the BCS, mean-field treatment. We note that, although here $\delta T(H)/T_c(H)$ for $p = 0.25 \pm 0.01$ appears to decrease towards zero as $T_c(H) \to 0$ (see highest $H$ in Fig. 1e) in agreement with general expectations for a phase transition driven by thermal fluctuations[40] at a fixed $H$, it is not possible to confirm the deviation from $\delta T(H)/T_c(H) \sim 2$ within error.

## Discussion

In charge- and spin-stripe-ordered $La_{1.875}Ba_{0.125}CuO_4$ (ref. 15), $La_{1.7}Eu_{0.2}Sr_{0.1}CuO_4$ and $La_{1.48}Nd_{0.4}Sr_{0.12}CuO_4$ (ref. 41), in which $p \approx 1/8$, the behavior with $R_H = 0$ and $\rho_{xx} \neq 0$ was observed in the viscous VL regime and thus attributed to the increasing viscosity of the vortex motion with decreasing $T$ (see also refs. 14,16). Most peculiarly, though, $R_H = 0$ with $\rho_{xx} \neq 0$ was found to persist over a large range of $T$ and $H$ in the high-field normal state[15,41], even with no evidence of any remnants of superconductivity[41]. While the precise origin of $R_H = 0$ in the normal state is still an open question, it may imply an approximate particle-hole symmetry that is unique to stripe-ordered cuprates. Indeed, our measurements on underdoped Bi-2201 reveal that the $R_H = 0$ with $\rho_{xx} \neq 0$ behavior is limited to the viscous VL, i.e., it is a signature of the SC regime with nearly frozen vortexlike phase fluctuations. These findings are reminiscent of $R_H = 0$ observed within the VL in some conventional disordered 2D superconductors[42,43] and oxide interfaces[44], as well as in $YBa_2Cu_3O_y$ thin films[45]. In those systems, however, $R_H = 0$ is found in the "anomalous metal regime" [42,43] with $\rho_{xx}(T \to 0) \neq 0$, in contrast to $\rho_{xx}(T \to 0) = 0$ in Bi-2201. It is interesting, though, that the vanishing of $R_H$ in such anomalous metals has been attributed[46] to the diluteness of mobile vortices due to strong pinning. In cuprates, it has also been suggested[47] that Berezinskii-Kosterlitz-Thouless-type (BKT) physics can give rise to $R_H = 0$ and $\rho_{xx} \neq 0$ just above $T_c$ due to the unbinding of vortex-antivortex pairs. In this scenario, a finite $\rho_{yx}$ appears only when a density of field-generated vortices becomes sufficiently large. However, we find that in the $R_H = 0$ regime above $T_c(H)$, $\rho_{xx}$ follows a simple power-law $T$-dependence (e.g., Supplementary Fig. 5a, b for the underdoped, and Supplementary Fig. 8 for the heavily overdoped region), in contrast to the exponential behavior characteristic of the ($H = 0$) BKT transition[48].

On general grounds, the most likely origin of strong pinning[35] that can give rise to $R_H = 0$ with $\rho_{xx} \neq 0$ in Bi-2201 is disorder. Disorder is expected to lead to emergent granular superconductivity[12,49], i.e., the inhomogeneity of the pairing amplitude on the scale of the coherence length, forming SC puddles weakly coupled by the Josephson effect. Although inhomogeneous, the pairing amplitude is finite throughout the system, and the SC transition occurs because of the loss of phase coherence. The presence of intrinsic electronic inhomogeneity, such as charge order, which in Bi-2201 extends to the heavily overdoped region[25,26], should enhance the tendency towards granularity and the importance of SC phase fluctuations further[43]. Scanning tunneling microscopy (STM) studies have indeed revealed evidence[50] for spatially inhomogeneous pairing gaps above $T_c^0$ in $Bi_2Sr_2CaCu_2O_{8+\delta}$ (Bi-2212) near optimal doping. At low doping, near the insulator-to-superconductor transition, both transport measurements[51] on $La_{2-x}Sr_xCuO_4$ and STM studies[52] on Bi-2201 have established that the onset of superconductivity, that is, of global phase coherence, is influenced by the competing charge order, and not merely by disorder. It is thus reasonable to speculate that, in heavily overdoped Bi-2201, both disorder and charge order may affect the value of $T_c^0$ and contribute to pinning responsible for $R_H = 0$ in the viscous VL regime. While identifying the precise origin and role of pinning in Bi-2201 is beyond the scope of this study, it is clear that the non-monotonic doping dependence of vortexlike phase fluctuations cannot be attributed solely to disorder. For example, even though in our weakly overdoped samples the disorder is much stronger than in the underdoped crystals (see "Methods"), the regime with $R_H = 0$ and $\rho_{xx} \neq 0$ is weakest. Likewise, it has been argued that the STM results[9], showing SC puddles above $T_c^0$ in heavily overdoped Bi-2201 and at even higher $p$, beyond the superconductor-to-metal transition, cannot be described entirely within the dirty $d$-wave scenario. This includes the extent in $T$ of pairing above $T_c^0$. Our finding of vortexlike phase fluctuations up to $\delta T(H \to 0)/T_c(H \to 0) \sim 7$ in heavily overdoped Bi-2201 (Fig. 1e) is consistent with the zero-field STM evidence from that study[9] for SC puddles and pairing up to $T \sim 7\,T_c^0$ in Bi-2201 single crystals with the same $p \approx 0.25$. The presence of Josephson-coupled SC grains has also been inferred[53] in heavily overdoped $La_{2-x}Sr_xCuO_4$. Similar to the predictions[12] for $H = 0$, the dirty $d$-wave (BCS) theory shows[54] that the interplay of disorder and orbital depairing by $H$ in hole-overdoped cuprates may lead to the emergence of an intermediate, granular regime with finite SC pairing and zero superfluid stiffness. Our observation of pronounced vortexlike excitations beyond the mean-field picture [$\delta T(H)/T_c(H) \gg 1$] in heavily overdoped Bi-2201 is qualitatively consistent with that scenario.

In summary, our comparative study of $T$–$H$ phase diagrams and low-$T$ magnetotransport properties in different doping regions of Bi-2201 using several complementary techniques has (a) demonstrated the universality of the vortex phase diagram in underdoped cuprates regardless of the presence of charge or spin orders, (b) indicated the persistence of pairing without phase coherence in an unusually wide range of $T$ above $T_c(H)$ in the heavily overdoped region, and (c) revealed that the importance of phase fluctuations in the SC transition depends on doping in a nonmonotonic fashion. While (b) and (c) were previously reported[30] in the $La_{2-x}Sr_xCuO_4$ family of cuprates based on the behavior of Gaussian fluctuations of the SC amplitude and phase (i.e., $H_c'(T)$ in our study) and correlated with a low superfluid density in both underdoped and overdoped regimes, our conclusions, in contrast, are based on the behavior of vortexlike excitations. Other experiments, such as STM studies in the presence of a magnetic field, are needed to provide further insight into the origin of the observed enhancement of vortexlike phase fluctuations in the heavily overdoped region, their relation to the strange metal regime[55], and the behavior of pairing amplitudes above $T_c(H)$. The strange metal has been indeed proposed[56] to arise from the scattering of quasiparticles from isolated SC puddles of strongly correlated electrons. Based on general arguments[40], our results strongly suggest that in sufficiently disordered, heavily overdoped cuprates at fixed $H$, the superconductor-to-metal transition (i.e., melting of the vortex lattice) at $T_c(H)$ is driven by thermal fluctuations. Quantum fluctuations, on the other hand, play a key role in the field-tuned destruction of superconductivity in the underdoped region as $T \to 0$ (i.e., in a quantum phase transition from a vortex glass to a normal state in Fig. 1b; also, refs. 14,16 for the La-214 family), but in heavily overdoped samples they are likely to become important only in the low-$T$, high-$H$ regime (cf. Fig. 1d, Fig. 1b, refs. 14,16) that is not accessible experimentally. The quantum superconductor-to-metal transition is not well understood in general[43], and thus further insight into the role of quantum fluctuations might actually come from similar experiments on unconventional superconductors that are simpler than cuprates, such as quasi-2D organic charge transfer salts[57,58].

## Methods

### Samples

Several Bi-2201 samples, both single crystals and thin films, covering underdoped, weakly overdoped, and heavily overdoped hole concentration regions were studied. In order to span such a wide range of doping levels, we have used three representative types of Bi-2201 subfamilies. The heavily overdoped thin film samples were prepared from the "pure" $Bi_2Sr_2CuO_{6+\delta}$ family, in which the carrier concentration is controlled solely by the oxygen content. However, unlike other cuprate systems such as $La_{2-x}Sr_xCuO_4$, $La_{2-x}Ba_xCuO_4$, or $YBa_2Cu_3O_{6+x}$, oxygen in this structure is relatively stable. As a result, it is difficult to significantly change the carrier concentration by post-annealing alone. Therefore, to vary the carrier density in the weakly overdoped region, we used the method of tuning the Bi:Sr nonstoichiometric ratio. This approach, however, has a limited doping range and cannot reach the underdoped region. To address this issue, we employed single crystals of La-doped Bi-2201 ($Bi_2Sr_{2-x}La_xCuO_{6+\delta}$), in which Sr is partially substituted with La to control the carrier concentration. This system is known to have a lower residual resistivity and to exhibit a significantly higher optimal $T_c^0$ ($T_{c,\,max}^0$) compared to the other two Bi-2201 subfamilies. Indeed, prior work has demonstrated that disorder due to (Sr, La) substitution is weaker than in the case of (Sr, Bi) substitution[20,59,60] because the ionic radius of $La^{3+}$ is more similar to that of $Sr^{2+}$ than the ionic radius of $Bi^{3+}$ (ref. 59).

Single crystals of underdoped Bi-2201, $Bi_2Sr_{1.16}La_{0.84}CuO_{6+\delta}$ (BSLCO) with $p \approx 0.10$, in which La substitution for Sr is used to control hole doping concentration, were grown using the floating-zone technique[20]. The maximum $T_c^0$ for the $Bi_2Sr_{2-x}La_xCuO_{6+\delta}$ family[20] is $T_{c,\,max}^0 \sim 38$ K for $p \sim 0.16$. Weakly overdoped $Bi_{2.1}Sr_{1.9}CuO_{6+\delta}$ ($p \approx 0.18$) single crystals were also grown by the floating-zone technique, with $T_{c,\,max}^0 \sim 10$ K for $Bi_{2+x}Sr_{2-x}CuO_{6+\delta}$ (refs. 59–61). Inductively coupled plasma spectroscopy was carried out to determine the chemical compositions of the crystals. The hole doping concentration for the underdoped crystal was determined[20] by comparing the Hall coefficient, normalized to the unit cell volume, to those of $La_{2-x}Sr_xCuO_4$ at different doping levels[62,63]. In weakly overdoped $Bi_{2+x}Sr_{2-x}CuO_{6+\delta}$ crystals, $p$ was determined by comparing the Hall coefficients to those of $Bi_2Sr_{2-x}La_xCuO_{6+\delta}$ (Supplementary Fig. 11a, b). In both cases, the uncertainty $\Delta p = \pm 0.02$ (refs. 62,63).

Although it has been argued recently that the widely used method of comparing the Hall coefficients of Bi-2201 to $La_{2-x}Sr_xCuO_4$ may not provide a reliable estimate of $p$, the question about a proper method to determine $p$ in Bi-2201 is still not fully resolved[22]. In ref. 21, $p$ was determined using the phenomenological formula proposed by Presland et al.[64]: $T_c^0/T_{c,\,max}^0 = 1 - 82.6(p-0.16)^2$. While the same formula with $T_{c,\,max}^0 \sim 10$ K predicts $p \approx 0.24$ for our $Bi_{2.1}Sr_{1.9}CuO_{6+\delta}$ crystal, a comparison of the Hall number per Cu atom $n_H \equiv V_{cell}/eR_H$ (here $V_{cell} = 3.8$ Å × 3.8 Å × 12.3 Å) obtained from our precise measurements at low $T$ and high fields ($n_H \approx 0.65$ from Supplementary Fig. 7b) to $n_H$ in ref. 21, yields $p \sim 0.20$. This apparent discrepancy is attributed to the uncertainty in $T_{c,\,max}^0$, which is known to depend strongly on the Bi:Sr ratio[59,60]. We note, however, that our main conclusions do not depend on the precise values of $p$, but only on the relative positions of our samples with respect to the pseudogap. Therefore, we have determined the pseudogap temperature $T_{PG}$ in $Bi_{2.1}Sr_{1.9}CuO_{6+\delta}$ from both the out-of-plane resistivity $\rho_c(T)$, as usual (see, e.g., ref. 65), and $\rho_{xx}(T)$ (see, e.g., ref. 21). Supplementary Fig. 11c, d shows that consistent values of $T_{PG} \sim 50$–$75$ K are obtained, placing our weakly overdoped crystal within the pseudogap region. According to ref. 22, in which $p$ in single crystals of $Bi_{2+z-y}Pb_ySr_{2-x-z}La_xCuO_{6+\delta}$ (Bi-2201) was found (to within $\Delta p = 0.01$) by comparing $\rho_{xx}(T)$ curves to those of $La_{2-x}Sr_xCuO_4$, $T_{PG} \sim 50$–$75$ K corresponds to $p \approx 0.20$, in a good agreement with $p = 0.18 \pm 0.02$ determined from the Hall coefficient (Supplementary Fig. 11a, b; also Supplementary Fig. 7b and ref. 21). Importantly, the pseudogap closes[22] at $p \sim 0.21$. For $p \approx 0.10$, the pseudogap temperature $T_{PG} \sim 250$ K (refs. 22,66).

The $p \approx 0.10$ and $p \approx 0.18$ samples were shaped as rectangular bars suitable for direct measurements of the longitudinal and transverse (Hall) resistivity, $\rho_{xx}$ and $\rho_{yx}$, respectively. Detailed measurements of $\rho_{xx}$ and $\rho_{yx}$ were performed on a $p \approx 0.10$ sample with dimensions $1.48 \times 0.87 \times 0.05$ mm$^3$ ($a \times b \times c$, i.e., length × width × thickness) and on a $p \approx 0.18$ sample with dimensions $1.27 \times 0.55 \times 0.03$ mm$^3$ ($a \times b \times c$). Both single crystal samples were measured in various systems, magnets and cryostats, over the period of ~3 years, and they were found to be stable and consistent in their behavior. The data are shown for the voltage contacts separated by 0.62 mm for $Bi_2Sr_{1.16}La_{0.84}CuO_{6+\delta}$ and 0.53 mm for $Bi_{2.1}Sr_{1.9}CuO_{6+\delta}$. The current contacts were painted to cover two opposing side faces of the platelet-shaped crystals to ensure a uniform current flow and the voltage contacts were painted on the two remaining side faces of the crystals. The contact pads were hand-drawn with gold paint, followed by a heat treatment at 400 °C for 30 min (i.e., for a week in case of a $p \approx 0.18$ crystal) in the air, which makes the gold particles adhere well to the sample surface. After this heat treatment to cure the gold contact pads, the samples were annealed in flowing air at 650 °C for 48 h to control the oxygen concentration, and they were quenched to room temperature at the end of the annealing. Finally, gold wires were attached to the contact pads using EPO-TEK® silver epoxy, which was cured at a relatively low temperature, 130 °C. The resulting contact resistances were less than 1 Ω at room temperature[20]. The out-of-plane resistivity $\rho_c$ shown in Supplementary Fig. 11d was measured on a $Bi_{2.1}Sr_{1.9}CuO_{6+\delta}$ ($p = 0.18 \pm 0.02$) sample, where the voltage contact distance was 0.053 mm (i.e., sample thickness along $c$) and the cross-sectional area was $0.91 \times 1.55$ mm$^2$. The sample was prepared by hand-painting ring-shaped current contacts and small circular voltage contacts in the center of the current-contact ring on the opposing $ab$ faces of the crystal[20]. The contacts were subsequently treated as described above.

Heavily overdoped thin films were prepared from the "pure" $Bi_2Sr_2CuO_{6+\delta}$ family by RF magnetron sputtering on $c$-axis oriented SrTiO3 single crystal substrates[67,68] and also on MgO substrates for composition analysis using Rutherford backscattering spectrometry[69]. (The values of $T_c^0$ are the same for both types of substrates.) Oxygen annealing treatments were used to control hole doping concentration. The films were patterned mechanically into Hall bars, parallel to the $a$ crystallographic axis, with six gold contacts for $\rho_{xx}$ and $\rho_{yx}$ measurements. Detailed measurements were performed on two heavily overdoped thin films: sample F2 with the actual cationic composition $Bi_{2.14}Sr_{1.86}Cu_{1.13}O_{6+\delta}$, dimensions $2 \times 0.365$ mm$^2$ ($a \times b$) and thickness of 310 nm, and sample F0 with the composition $Bi_{2.15}Sr_2Cu_{1.16}O_{6+\delta}$, dimensions $2 \times 0.332$ mm$^2$ ($a \times b$) and thickness of 78 nm. The data are shown for the voltage contacts separated by 0.62 mm for the F2 sample and 0.61 mm for the F0 sample. The hole concentrations determined using the Presland et al. formula[64] with $T_{c,\,max}^0 = (16 \pm 2)$ K (refs. 67–70) were $p \approx 0.26$ and $p \approx 0.27$ for samples F2 and F0, respectively. However, the Hall number $n_H \approx 0.8$ obtained for sample F2 (Supplementary Fig. 10b) corresponds to the hole concentration of ~0.24 in ref. 21, which also used the Presland et al. formula[64] to determine $p$. Therefore, we conclude that $p = 0.25 \pm 0.01$ for sample F2, with at least the same uncertainty $\Delta p = \pm 0.01$ for sample F0 ($p \approx 0.27$).

For each sample, $T_c^0$ was defined as the temperature at which the linear resistivity becomes zero, i.e., falls below the experimental noise floor (~0.7 mΩ), giving $T_c^0 = (1.8 \pm 0.2)$ K for $p \approx 0.10$, $T_c^0 = (4.8 \pm 0.3)$ K for $p \approx 0.18$, $T_c^0 = (3.3 \pm 0.2)$ K for $p \approx 0.25$, and $T_c^0 < 0.4$ K for $p \approx 0.27$ ($T = 0.4$ K was the lowest measurement temperature for this sample).

### Measurements

The standard four-probe ac method (~13 Hz) was used for measurements of the longitudinal and transverse resistances, $R_{xx}$ and $R_{yx}$, respectively, with the magnetic field parallel and antiparallel to the $c$

axis. The Hall resistance was determined from the transverse voltage by extracting the component antisymmetric in the magnetic field. The Hall coefficient $R_H = R_{yx}\, d/H = \rho_{yx}/H$, where $d$ is the sample thickness. The resistance per square per $CuO_2$ layer $R_{\square/layer} = \rho_{xx}/l$, where $l = 12.3$ Å is the spacing between layers. (The ~2% error introduced into the calculation of $R_{\square/layer}$ for $Bi_2Sr_{1.16}La_{0.84}CuO_{6+\delta}$ by taking $l = 12.3$ Å instead of the more precise[68] $l \approx 12.0$ Å is negligible compared to the ~30% geometrical uncertainty in $\rho_{xx}$, typical of cuprate samples[22], and it does not affect any of our conclusions.) Depending on the temperature and magnetic field, the excitation current (density) of 1 μA to 100 μA ($2.3 \times 10^{-3}$ A/cm$^2$ to 0.230 A/cm$^2$ for $p \approx 0.10$ sample and $6 \times 10^{-3}$ A/cm$^2$ to 0.606 A/cm$^2$ for $p \approx 0.18$ sample) was used for the single crystals, and 100 nA to 300 nA (0.088 A/cm$^2$ to 0.265 A/cm$^2$) for thin films. The excitation currents were adjusted to ensure Ohmic behavior, i.e., to avoid Joule heating. $dV/dI$ measurements were performed by applying a dc current bias $I_{dc}$ and a small ac current excitation $I_{ac}$ (~13 Hz) through the sample while measuring the ac voltage across the sample. For each value of $I_{dc}$, the ac voltage was monitored for 300 s, and the average value was recorded[16,39]. A 1 kΩ resistor in series with a $\pi$ filter [5 dB (60 dB) noise reduction at 10 MHz (1 GHz)] was placed in each wire at the room temperature end of the cryostat to reduce the noise and heating by radiation in all measurements.

The experiments were conducted in several different magnets at the National High Magnetic Field Laboratory: a dilution refrigerator ($0.016\ K \leqslant T \leqslant 1.1\ K$) in superconducting magnets with $H$ up to 18 T and 28 T, and a $^3$He system ($0.3\ K \leqslant T \leqslant 60\ K$) in a superconducting magnet with $H$ up to 18 T, using 0.1–0.2 T/min sweep rates; a $^3$He system ($0.3\ K \leqslant T \leqslant 15\ K$) in a 35 T resistive magnet, using 1–2 T/min sweep rate; a $^3$He system ($0.3\ K \leqslant T \leqslant 30\ K$) in a 41 T resistive magnet, using 1 T/min sweep rate; and a $^3$He system ($0.3\ K \leqslant T \leqslant 12\ K$) in a 45 T hybrid magnet, using 1–2 T/min sweep rates. The fields were swept at constant temperatures, and the sweep rates were low enough to avoid eddy current heating of the samples. The results obtained in different magnets and cryostats agree well.

## Data availability

The data that support the findings of this study are included in the article and its Supplementary Information. Source data are provided with this paper.

## References


1. Uemura, Y. J. et al. Universal correlations between $T_c$ and $n_s/m^*$ (carrier density over effective mass) in high-$T_c$ cuprate superconductors. *Phys. Rev. Lett.* **62**, 2317–2320 (1989).
2. Emery, V. & Kivelson, S. Importance of phase fluctuations in superconductors with small superfluid density. *Nature* **374**, 434–437 (1995).
3. Lee, P. A., Nagaosa, N. & Wen, X.-G. Doping a Mott insulator: Physics of high-temperature superconductivity. *Rev. Mod. Phys.* **78**, 17–85 (2006).
4. Keimer, B., Kivelson, S. A., Norman, M. R., Uchida, S. & Zaanen, J. From quantum matter to high-temperature superconductivity in copper oxides. *Nature* **518**, 179–186 (2015).
5. Larkin, A. & Varlamov, A. *Theory of Fluctuations in Superconductors* (Oxford University Press, Oxford, 2009).
6. Božović, I., He, X., Wu, J. & Bollinger, A. T. Dependence of the critical temperature in overdoped copper oxides on superfluid density. *Nature* **536**, 309–311 (2016).
7. Mahmood, F., He, X., Božović, I. & Armitage, N. P. Locating the missing superconducting electrons in the overdoped cuprates $La_{2-x}Sr_xCuO_4$. *Phys. Rev. Lett.* **122**, 027003 (2019).
8. He, Y. et al. Superconducting fluctuations in overdoped $Bi_2Sr_2CaCu_2O_{8+\delta}$. *Phys. Rev. X* **11**, 031068 (2021).
9. Tromp, W. O. et al. Puddle formation and persistent gaps across the non-mean-field breakdown of superconductivity in overdoped $(Pb,Bi)_2Sr_2CuO_{6+\delta}$. *Nat. Mater.* **22**, 703–709 (2023).
10. Lee-Hone, N. R., Özdemir, H. U., Mishra, V., Broun, D. M. & Hirschfeld, P. J. Low energy phenomenology of the overdoped cuprates: viability of the Landau-BCS paradigm. *Phys. Rev. Res.* **2**, 013228 (2020).
11. Pal, M., Kreisel, A., Atkinson, W. A. & Hirschfeld, P. J. Simulating superconducting properties of overdoped cuprates: the role of inhomogeneity. *Phys. Rev. B* **107**, 144501 (2023).
12. Li, Z.-X., Kivelson, S. A. & Lee, D.-H. Superconductor-to-metal transition in overdoped cuprates. *npj Quantum Mater.* **6**, 36 (2021).
13. Sous, J., He, Y. & Kivelson, S. A. Absence of a BCS-BEC crossover in the cuprate superconductors. *npj Quantum Mater.* **8**, 25 (2023).
14. Shi, X., Lin, P. V., Sasagawa, T., Dobrosavljević, V. & Popović, D. Two-stage magnetic-field-tuned superconductor-insulator transition in underdoped $La_{2-x}Sr_xCuO_4$. *Nat. Phys.* **10**, 437–443 (2014).
15. Li, Y. et al. Tuning from failed superconductor to failed insulator with magnetic field. *Sci. Adv.* **5**, eaav7686 (2019).
16. Shi, Z., Baity, P. G., Sasagawa, T. & Popović, D. Vortex phase diagram and the normal state of cuprates with charge and spin orders. *Sci. Adv.* **6**, eaay8946 (2020).
17. Li, Q., Hucker¨, M., Gu, G. D., Tsvelik, A. M. & Tranquada, J. Two-dimensional superconducting fluctuations in stripe-ordered $La_{1.875}Ba_{0.125}CuO_4$. *Phys. Rev. Lett.* **99**, 067001 (2007).
18. Baity, P. G., Shi, X., Shi, Z., Benfatto, L. & Popović, D. Effective two-dimensional thickness for the Berezinskii-Kosterlitz-Thouless-like transition in a highly underdoped $La_{2-x}Sr_xCuO_4$. *Phys. Rev. B* **93**, 024519 (2016).
19. Ding, Y. et al. Disappearance of superconductivity and a concomitant Lifshitz transition in heavily overdoped $Bi_2Sr_2CuO_6$ superconductor revealed by angle-resolved photoemission spectroscopy. *Chin. Phys. Lett.* **36**, 017402 (2019).
20. Ono, S. & Ando, Y. Evolution of the resistivity anisotropy in $Bi_2Sr_{2-x}La_xCuO_{6+\delta}$ single crystals for a wide range of hole doping. *Phys. Rev. B* **67**, 104512 (2003).
21. Putzke, C. et al. Reduced Hall carrier density in the overdoped strange metal regime of cuprate superconductors. *Nat. Phys.* **17**, 826–831 (2021).
22. Berben, M. et al. Superconducting dome and pseudogap endpoint in Bi2201. *Phys. Rev. Mater.* **6**, 044804 (2022).
23. Juskus, D., Ayres, J., Nicholls, R. & Hussey, N. E. Insensitivity of $T_c$ to the residual resistivity in high-$T_c$ cuprates and the tale of two domes. *Front. Phys.* **12**, 1396463 (2024).
24. Peng, Y. Y. et al. Direct observation of charge order in underdoped and optimally doped $Bi_2(Sr, La)_2CuO_{6+\delta}$ by resonant inelastic x-ray scattering. *Phys. Rev. B* **94**, 184511 (2016).
25. Peng, Y. Y. et al. Re-entrant charge order in overdoped (Bi, $Pb)_{2.12}Sr_{1.88}CuO_{6+\delta}$ outside the pseudogap regime. *Nat. Mater.* **17**, 697–702 (2018).
26. Li, X. et al. Evolution of charge and pair density modulations in overdoped $Bi_2Sr_2CuO_{6+\delta}$. *Phys. Rev. X* **11**, 011007 (2021).
27. Peng, Y. Y. et al. Dispersion, damping, and intensity of spin excitations in the monolayer $(Bi, Pb)_2(Sr,La)_2CuO_{6+\delta}$ cuprate superconductor family. *Phys. Rev. B* **98**, 144507 (2018).
28. Ono, S. et al. Metal-to-insulator crossover in the low-temperature normal state of $Bi_2Sr_{2-x}La_xCuO_{6+\delta}$. *Phys. Rev. Lett.* **85**, 638–641 (2000).
29. Rullier-Albenque, F. et al. Total suppression of superconductivity by high magnetic fields in $YBa_2Cu_3O_{6.6}$. *Phys. Rev. Lett.* **99**, 027003 (2007).
30. Rourke, P. M. C. et al. Phase-fluctuating superconductivity in overdoped $La_{2-x}Sr_xCuO_4$. *Nat. Phys.* **7**, 455–458 (2011).

31. Balakirev, F. F. et al. Signature of optimal doping in Hall-effect measurements on a high-temperature superconductor. *Nature* **424**, 912–915 (2003).
32. Fisher, M. P. A. Vortex-glass superconductivity: A possible new phase in bulk high-$T_c$ oxides. *Phys. Rev. Lett.* **62**, 1415–1418 (1989).
33. Fisher, D. S., Fisher, M. P. A. & Huse, D. A. Thermal fluctuations, quenched disorder, phase transitions, and transport in type-II superconductors. *Phys. Rev. B* **43**, 130–159 (1991).
34. Dorsey, A. T., Huang, M. & Fisher, M. P. A. Dynamics of the normal to vortex-glass transition: mean-field theory and fluctuations. *Phys. Rev. B* **45**, 523–526 (1992).
35. Le Doussal, P. Novel phases of vortices in superconductors. *Int. J. Mod. Phys. B* **24**, 3855–3914 (2010).
36. Fisher, M. P. A. Quantum phase transitions in disordered two-dimensional superconductors. *Phys. Rev. Lett.* **65**, 923–926 (1990).
37. Ando, Y., Boebinger, G. S., Passner, A., Kimura, T. & Kishio, K. Logarithmic divergence of both in-plane and out-of-plane normal-state resistivities of superconducting $La_{2-x}Sr_xCuO_4$ in the zero-temperature limit. *Phys. Rev. Lett.* **75**, 4662–4665 (1995).
38. Hsu, Y.-T. et al. Anomalous vortex liquid in charge-ordered cuprate superconductors. *Proc. Natl. Acad. Sci. USA* **118**, e2016275118 (2021).
39. Shi, Z., Baity, P. G., Terzic, J., Sasagawa, T. & Popović, D. Pair density wave at high magnetic fields in cuprates with charge and spin orders. *Nat. Commun.* **11**, 3323 (2020).
40. Sachdev, S. *Quantum Phase Transitions* (Cambridge University Press, 2011).
41. Shi, Z. et al. Magnetic field reveals vanishing Hall response in the normal state of stripe-ordered cuprates. *Nat. Commun.* **12**, 3724 (2021).
42. Breznay, N. P. & Kapitulnik, A. Particle-hole symmetry reveals failed superconductivity in the metallic phase of two-dimensional superconducting films. *Sci. Adv.* **3**, e1700612 (2017).
43. Kapitulnik, A., Kivelson, S. A. & Spivak, B. Colloquium: anomalous metals: failed superconductors. *Rev. Mod. Phys.* **91**, 011002 (2019).
44. Chen, Z. et al. Universal behavior of the bosonic metallic ground state in a two-dimensional superconductor. *npj Quantum Mater.* **6**, 15 (2021).
45. Yang, C. et al. Intermediate bosonic metallic state in the superconductor-insulator transition. *Science* **366**, 1505–1509 (2019).
46. Delacrétaz, L. V. & Hartnoll, S. A. Theory of the supercyclotron resonance and Hall response in anomalous two-dimensional metals. *Phys. Rev. B* **97**, 220506(R) (2018).
47. Yang, F., Shi, Y. & Chen, L.-Q. Preformed Cooper pairing and the uncondensed normal-state component in phase-fluctuating cuprate superconductivity. Preprint at https://arxiv.org/abs/2509.21133 (2025).
48. Halperin, B. I. & Nelson, D. R. Resistive transition in superconducting films. *J. Low Temp. Phys.* **36**, 599–616 (1979).
49. Bouadim, K., Loh, Y. L., Randeria, M. & Trivedi, N. Single- and two-particle energy gaps across the disorder-driven superconductor-insulator transition. *Nat. Phys.* **7**, 884–889 (2011).
50. Pasupathy, A. N. et al. Electronic origin of the inhomogeneous pairing interaction in the high-$T_c$ superconductor $Bi_2Sr_2CaCu_2O_{8+\delta}$. *Science* **320**, 196–201 (2008).
51. Shi, X. et al. Emergence of superconductivity from the dynamically heterogeneous insulating state in $La_{2-x}Sr_xCuO_4$. *Nat. Mater.* **12**, 47–51 (2013).
52. Ye, S. et al. The emergence of global phase coherence from local pairing in underdoped cuprates. *Nat. Phys.* **19**, 1301–1308 (2023).
53. Li, Y. et al. Strongly overdoped $La_{2-x}Sr_xCuO_4$: evidence for Josephson-coupled grains of strongly correlated superconductor. *Phys. Rev. B* **106**, 224515 (2022).
54. Johnsen, L. G. The magnetic field driven superconductor-metal transition in disordered hole-overdoped cuprates. *J. Phys. Condens. Matter* **35**, 115601 (2023).
55. Ayres, J. et al. Universal correlation between *H*-linear magnetoresistance and *T*-linear resistivity in high-temperature superconductors. *Nat. Commun.* **15**, 8406 (2024).
56. Tranquada, J. M., Lozano, P. M., Yao, J., Gu, G. D. & Li, Q. From nonmetal to strange metal at the stripe-percolation transition in $La_{2-x}Sr_xCuO_4$. *Phys. Rev. B* **109**, 184510 (2024).
57. Pustogow, A. et al. Rise and fall of Landau's quasiparticles while approaching the Mott transition. *Nat. Commun.* **12**, 1571 (2021).
58. Wang, Y. et al. Failed superconductivity in a Mott spin liquid material. Preprint at https://arxiv.org/abs/2507.10832 (2025).
59. Eisaki, H. et al. Effect of chemical inhomogeneity in bismuth-based copper oxide superconductors. *Phys. Rev. B* **69**, 064512 (2004).
60. Vedeneev, S. I. & Maude, D. K. Metal-to-insulator crossover and pseudogap in single-layer $Bi_{2+x}Sr_{2-x}Cu_{1+y}O_{6+\delta}$ single crystals in high magnetic fields. *Phys. Rev. B* **70**, 184524 (2004).
61. Luo, H. & Wen, H.-H. Localization of charge carriers in the normal state of underdoped $Bi_{2+x}Sr_{2-x}CuO_{6+\delta}$. *Phys. Rev. B* **89**, 024506 (2014).
62. Ando, Y. et al. Carrier concentrations in $Bi_2Sr_{2-z}La_zCuO_{6+\delta}$ single crystals and their relation to the Hall coefficient and thermopower. *Phys. Rev. B* **61**, R14956–14959 (2000).
63. Ando, Y. et al. Erratum: Carrier concentrations in $Bi_2Sr_{2-z}La_zCuO_{6+\delta}$ single crystals and their relation to the Hall coefficient and thermopower. *Phys. Rev. B* **63**, 069902 (2001).
64. Presland, M. R., Tallon, J. L., Buckley, R. G., Liu, R. S. & Flower, N. E. General trends in oxygen stoichiometry effects on $T_c$ in Bi and Tl superconductors. *Phys. C* **176**, 95–105 (1991).
65. Katterwe, S. O., Jacobs, T. H., Maljuk, A. & Krasnov, V. M. Low anisotropy of the upper critical field in a strongly anisotropic layered cuprate $Bi_{2.15}Sr_{1.9}CuO_{6+\delta}$: evidence for a paramagnetically limited superconductivity. *Phys. Rev. B* **89**, 214516 (2014).
66. He, Y. et al. Rapid change of superconductivity and electron-phonon coupling through critical doping in Bi-2212. *Science* **362**, 62–65 (2018).
67. Li, Z. Z., Rifi, H., Vaures, A., Megtert, S. & Raffy, H. Oxygen-induced superconducting, metallic or insulating behaviour in as-grown epitaxial $Bi_2Sr_2CuO_x$ thin films. *Phys. C* **206**, 367–372 (1993).
68. Li, Z. Z., Raffy, H., Bals, S., van Tendeloo, G. & Megtert, S. Interplay of doping and structural modulation in superconducting $Bi_2Sr_{2-x}La_xCuO_{6+\delta}$ thin films. *Phys. Rev. B* **71**, 174503 (2005).
69. Raffy, H., Li, Z. Z. & Auban-Senzier, P. Transport properties of very overdoped nonsuperconducting $Bi_2Sr_2CuO_{6+\delta}$ thin films. *Phys. Rev. B* **106**, 224503 (2022).
70. Konstantinović, Z. et al. Failure of the empirical OCT law in the $Bi_2Sr_2CuO_{6+\delta}$ compound. *Europhys. Lett.* **62**, 257–263 (2003).


## Acknowledgements

We acknowledge P. G. Baity and L. J. Stanley for technical support, and S. A. Kivelson, J. M. Tranquada for helpful discussions. This work was supported by NSF Grants Nos. DMR-1707785 (D. P.) and DMR-2104193 (D. P.), and the National High Magnetic Field Laboratory through the NSF Cooperative Agreement Nos. DMR-1644779 and DMR-2128556, and the State of Florida. This research was also supported in part by the National Science Foundation under Grants No. NSF PHY-1748958 and PHY-2309135. S. O. acknowledges support from the JSPS KAKENHI grant (20H05304).

## Author contributions

Single crystals were grown and prepared by S.O.; thin films were grown and prepared by Z.Z.L. and H.R.; J.T., B.K.P., P.S., and H. R. performed the measurements; J.T. and B.K.P. analyzed the data; J.T., B.K.P., and D.P.

wrote the manuscript, with input from all authors; D.P. planned and supervised the investigation.

## Competing interests
The authors declare no competing interests.

## Additional information
**Supplementary information** The online version contains supplementary material available at https://doi.org/10.1038/s41467-025-67503-z.

**Correspondence** and requests for materials should be addressed to Dragana Popović.

**Peer review information** *Nature Communications* thanks the anonymous reviewers for their contribution to the peer review of this work. A peer review file is available.